LANGMUIR

pubs.acs.org/Langmuir Article

Protein Corona on Gold Nanoparticles Studied with Coarse-Grained Simulations

Md Symon Jahan Sajib, Pranab Sarker, Yong Wei,* Xiuping Tao,* and Tao Wei*

Cite This: *Langmuir* 2020, 36, 13356–13363 Read Online

ACCESS | Metrics & More | Article Recommendations | Supporting Information

ABSTRACT: Understanding protein corona formation in an aqueous environment at the molecular and atomistic levels is critical to applications such as biomolecule-detection and drug delivery. In this work, we employed mesoscopic coarse-grained simulations to study ovispirin-1 and lysozyme protein coronas on bare gold nanoparticles. Our study showed that protein corona formation is governed by protein−surface and protein−protein interactions, as well as the surface hydrophobic effect. The corona structure was found to be dependent on protein types and the size of nanoparticles. Ovispirin proteins form homogeneous single-layered adsorption in comparison with the lysozyme's inhomogeneous multilayered aggregates on gold NP surfaces. The decrease in nanoparticle size leads to more angular degrees of freedom for protein adsorption orientation. Subsequent atomistic molecular dynamics simulations further demonstrate the loss of secondary structure of ovispirin upon adsorption and the heterogeneity of its local structure.

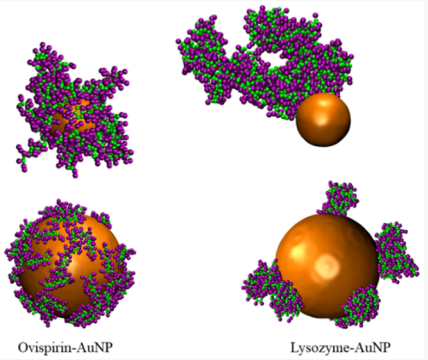

INTRODUCTION

Nanosized engineered particles using metals, such as gold and silver, possess unique electronic and optical properties, high surface-to-volume ratio, biocompatibility, and ease and consistency in synthesis.[1−5] It is well-known that the exposure of a nanoparticle (NP) to biological fluids leads to adsorption of multiple proteins, i.e., the formation of protein corona.[6−10] Previous studies[11−13] showed that a small amount of proteins (<5 ng cm^{-2}) adsorbed on the NP surface, that is, the formation of protein corona, can result in alteration of the chemicophysical and biological properties of the NP surface and subsequent propagation of biofouling through the attachment of biomolecules and microorganisms. For example, protein corona covering metallic AuNP surfaces leads to the red-shift of the surface plasmon resonance peak and a change in the NP surface charge and hydrodynamic diameter.[14] Fundamental understanding of NP−protein interactions and the formation of the protein corona on NP surfaces is critical to the development of novel detection devices, such as SERS[15,16] with high sensitivity and selectivity for disease detection, and is also very important to the design of new antibiofouling materials[11,17,18] that resist protein adsorption and the attachment of microorganisms for the marine industry[19] or nanomedicine research.[20]

As pristine NPs do not interact directly with living cells, the protein corona mediates such interactions, and its composition determines the biological identity, interactions, biological fate, and pharmacokinetics of the injected NPs.[21] Upon entering biological systems, a corona, i.e., the adsorption of proteins usually at higher concentrations, forms in less than 0.5 min.[22] During corona formation, the NP can alter the structure of the adsorbed proteins on its surface, setting off protein denaturation or significant conformational changes and, eventually, the concomitant loss of their biological function. Several factors, such as the composition, size, and shape of the injected NPs, ligand coating, time of exposure, nature of the physiological environment, the amounts of NPs and proteins, and protein affinity to NPs, influence the composition and features of the protein corona.[23,24] Therefore, understanding the process of the formation and the properties of protein corona on nanoparticles is essential to control their bioidentity, signaling, kinetics, transport, accumulation, and toxicity of drug-carrier NPs. Knowledge of such information beforehand will guide the safer and more efficient use of NPs across various applications.

Despite continuous efforts on the experimental front,[8,14,25−27] an in-depth understanding of the NP corona formation, particularly at the atomistic and molecular scale, is still highly desired. This is primarily due to the inherent complexity of the NP and biomolecules themselves and the experimental dilemma[8,25] in the ability to measure without perturbing the original corona in an aqueous environment. Under this circumstance, computer-aided simulations are great alternative tools that can complement experimental under-

Received: September 21, 2020
Revised: October 13, 2020
Published: October 30, 2020

https://dx.doi.org/10.1021/acs.langmuir.0c02767
Langmuir 2020, 36, 13356−13363

standing. For example, computationally expensive atomistic molecular dynamics (MD) simulations enable the exploration of the molecular details of protein adsorption at the surface−water interfaces.[28−37] Coarse-grained (CG) MD can model protein interfacial behavior at the mesoscopic scale with significant efficiency by lowering the resolution representation, where a number of atoms are simplified as a CG particle, and by simplifying the intramolecular interaction functions.[38−41]

A recent study[42] using CGMD simulation showed that on hydrophilic silica NP surfaces having increasing size (i.e., decreasing surface curvature), the adsorbed lysozyme showed a narrower orientation distribution on a hydrophilic silica NP due to stronger water−NP interactions.[42] According to Lopez and Lobaskin,[43] the curvature of the NP plays an important role in determining the sections of a human blood plasma protein that would be in contact with the NP surface. In contrast, Tavanti and co-workers did not find[44] a significant role of the NP size effect in ubiquitin protein−NP binding modalities. Further studies are desired to understand and confirm the dynamic process of the protein corona formation, protein−NP interactions, corona stability, and the overall composition of the protein corona, which is the motivation for this current work.

In this study, using efficient CGMD simulations at the mesoscopic scale, we studied the corona formation and specific properties including protein binding modalities, the interaction between protein and AuNP, and the change in protein structure upon adsorption on hydrophobic bare AuNP surfaces. In addition, classical atomistic MD simulations were performed to examine the protein structural changes upon adsorption on surfaces of AuNPs. Two differently sized AuNPs and proteins, ovispirin-1 and lysozyme, were used as model systems to investigate the formation and packing structure of the protein corona, as well as effects of nanoparticle size and protein types. Such fundamental research will be crucial to the future development of biosensing techniques such as SERS using gold nanoparticles, nanomedicine, and biomaterials.

METHODS

As a first step, we performed large-scale CGMD simulations to study the initial adsorption of multiple proteins on AuNP surfaces. The MARTINI 3.0 force field[45] was chosen in CGMD, as it offers improvement in excessive protein aggregation and water freezing problems, which were commonplace in the old version of the MARTINI force field. The Martini force field does not allow for changes of the protein secondary structure, which is imposed by an elastic network connecting the CG beads. In the second step, to study the denaturation of the adsorbed proteins, atomistic MD simulations were performed using the CHARMM36 force field.[46] Both CG and atomistic MD simulations were carried out using GROMACS[47] (Version 5.1.2), with the help of the mapping and reverse-mapping python script[48] to convert structures from all-atoms (MD) to beads (CG) and vice versa. Atoms of the AuNP were fixed at their initial position to immobilize the entire nanoparticle.

CGMD Simulations. Protein CG structures were derived from all-atom models which were obtained from the protein data bank (pdb codes: 1HU5 for ovispirin-1 and 1HWA for lysozyme), according to the MARTINI 3.0 force field which can be available from the Martini web portal.[49] The all-atom models were then transferred to the corresponding CG models with harmonic distance restraints on the backbone particles to maintain the protein's secondary structures. The lysozyme model consists of 291 CG beads, and the ovispirin model includes 47 CG beads. A single CG ovispirin model has a charge of +7, while a single lysozyme CG structure has a charge of +8. The MARTINI force field[45] incorporates bonded interactions and nonbonded interactions, the latter of which consist of the Lennard−Jones (LJ) and electrostatic potentials. The LJ interaction with a shifted 12-6 potential with a cutoff of 1.1 nm is represented as,

$$U_{\mathrm{LJ}}(r_{ij}) = 4\varepsilon_{ij}\left[\left(\frac{\sigma_{ij}}{r_{ij}}\right)^{12} - \left(\frac{\sigma_{ij}}{r_{ij}}\right)^{6}\right] \quad (1)$$

where r_{ij}, σ_{ij}, and ε_{ij} are the distance, the effective bead size, and the strength of the interaction between two beads i and j, respectively. The value of σ_{ij} is 0.47 nm for the interactions of all CG beads, except for the charged or apolar beads with σ_{ij} = 0.62 nm. Depending on the bead types, ε_{ij} is within the range of 2.0−5.6 kJ/mol. In experimental synthesis, AuNP surfaces can be hydrophilic due to oxidation or contamination dependent on the fabrication methodology.[50] However, in our simulation, a bare AuNP was directly cut from the gold lattice without consideration of surface oxidation and contamination. Such an ideal model of AuNPs being hydrophobic in nature has been widely adopted in previously published simulation papers[51−54] as well. In our model, an AuNP was presented with an atomistic description, each atom of which was assigned a MARTINI C5-type hydrophobic CG bead by following the previous papers.[51−54] All the σ_{ij} and ε_{ij} values for C5-type beads were adopted to describe the interaction of AuNP particles depending on the other interacting particles. The interactions between the CG beads of protein with water were represented with an LJ potential with parameters (σ = 0.2569 nm, ϵ = 4.19 kJ/mol) and the standard Lorentz−Berthelot mixing rule.[53,55,56] The Columbic potential of protein charged groups are with the 1.1 nm cutoff,

$$U_{\mathrm{ele}}(r_{ij}) = \frac{q_i q_j}{4\pi\epsilon_0\epsilon_r r_{ij}} \quad (2)$$

where q_i and q_j are the charges of beads i and j, respectively, ϵ_0 is the dielectric constant in vacuum, and ϵ_r is the relative dielectric constant.

A total of 44 ovispirin proteins were assembled with 3.2 and 10 nm AuNPs in two simulation boxes of different sizes (26 × 26 × 26 nm^3 for the 3.2 nm AuNP and 26.3 × 26.3 × 26.3 nm^3 for the 10 nm AuNP) so that the ovispirin mass concentration remained the same for both NPs. Proteins were solvated with water of the MARTINI standard model, where one solvent CG bead represents four water molecules. Counterions were added to neutralize the systems. A similar protocol of assembling, solvation, and charge neutralization was also used for seven lysozyme proteins placed on 3.2 and 10 nm AuNPs.

All the simulations were carried out using NVT ensembles with periodic boundary conditions (PBC). The nonbonded neighbors' list was updated every 20 steps, using the verlet cutoff scheme. The temperature of the proteins, NPs, water, and ions was coupled separately using a velocity-rescale[57] thermostat at 300 K. We chose a time step of 20 fs for the integration of the equation of beads' motion.

Atomistic MD Simulations. In the atomistic MD simulation, we investigated the structural change of 44 ovispirin proteins after the formation of corona on the 10

https://dx.doi.org/10.1021/acs.langmuir.0c02767
Langmuir 2020, 36, 13356−13363

nm AuNP surface. Each atomistic model of ovispirin has a charge of +7. CHARMM36[46] was used to model protein bonded and nonbonded interactions, and the TIP3P water model was adopted. The Au−protein and Au−water atomistic interactions were modeled with the LJ potential obtained from the literature.[58,59] The final CG configuration at 5.6 μs was taken to obtain the atomistic structure through reverse mapping as an input for the subsequent atomistic MD simulations.

All proteins on the NP surfaces were included in atomistic simulations except unadsorbed proteins in a smaller box to reduce the computational load in atomistic MD simulations. In the atomistic MD simulations, the all-atom structure was assembled with a 10 nm AuNP, the adsorbed proteins, and water molecules in a simulation box of 15.94 × 15.94 × 15.94 nm^3 with the PBC condition. Counterions were added to make the system neutral. The whole system was initially equilibrated in an NVT ensemble at 298.15 K with the thermostat method of the velocity rescale, keeping all proteins constrained. Then the proteins were allowed to relax freely, and the system was further equilibrated in an NPT ensemble at 1 bar for another 93 ns, using the Parrinello−Rahman method. The leapfrog algorithm was adopted to integrate the dynamics with a time step of 1 fs in the atomistic MD. For the long-range electrostatic interactions, the Particle Mesh Ewald summation was utilized, with a cutoff distance of 1.2 nm for separating the direct and reciprocal space. The same cutoff for the LJ potential was set, and the long-range dispersion effect on energy and pressure was applied.

RESULTS

Formation and Structure of the Ovispirin Protein Corona. To facilitate the entry of nucleus-targeting medical agents into cell nuclei, drug molecules or nanomaterials need to be smaller than the pore size (9−12 nm) of nuclear pore complexes.[20,60] Moreover, for the purpose of achieving high sensitivity of molecular detection using local surface plasmon resonance spectrum effects for the SERS technique, the sizes of nanoparticles are usually in the range of 10−100 nm. To facilitate future development of nanomedicine, biomaterials, and the SERS technique, in this work, we chose AuNPs of two different sizes (3.2 and 10 nm) to study their interactions with proteins. Figure 1 shows the dynamic processes of ovispirin corona formation on both AuNP surfaces. In our CGMD simulations, proteins were initially randomly distributed in the bulk water with the same initial protein concentration for both cases of different sized nanoparticles (Figure 1a,d). The dynamics of ovispirin corona formation displayed a similar pattern on both AuNP surfaces. Within the first 1.4 μs, a few ovispirin proteins were adsorbed on the AuNP surface rapidly (Figure 1b,e). Then the rest of the ovispirin proteins competed for the bare AuNP surface to secure a spot for landing. Upon obtaining a landing spot, they reorient themselves to complete the adsorption process and form the first adsorption layer on both NP surfaces due to the strong protein−surface interactions. On the surface of the 3.2 nm AuNP, 17 proteins out of a total of 44 were observed to remain in bulk after the completion of the first layer of corona (Figure 1c). In contrast, on the 10 nm AuNP surface, all proteins in the bulk water were adsorbed onto the NP surface (Figure 1f) due to a larger surface area available for protein−surface interactions. The formation of the first adsorption layer of ovispirin on the 3.2 nm AuNP was completed within 1.5 μs (Figure 1a−c), while

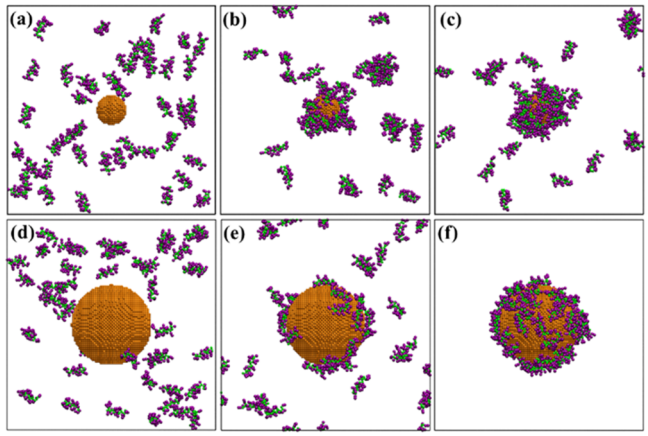

Figure 1. Dynamic processes of the formation of the ovispirin corona on the surface of a 3.2 nm AuNP ((a) the initial; (b) at t = 1 μs; (c) at t = 19 μs), and on a 10 nm AuNP ((d) the initial; (e) t = 1 μs; (f) t = 5.6 μs)).

the second or upper layer(s) was barely observed. Within 5.9 μs in our simulation, only one ovispirin was observed to position itself on the top of other proteins. Slight aggregations of ovispirin proteins were observed in bulk prior to corona formation in both cases. After the first-layer corona was formed, a few ovispirin clusters were detected in bulk in the case of the smaller 3.2 nm NP.

To further examine the case of 3.2 nm NPs, we calculated their density distribution in the radial direction $\rho(r)$ (bead no./nm^3) (see Figure 2),

$$\rho(r) = \frac{n}{4\pi r^2 dr} \tag{3}$$

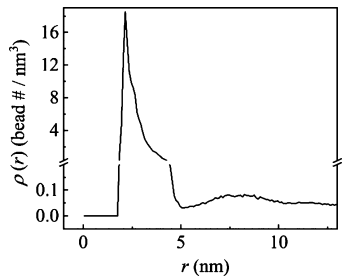

Figure 2. Radial density distribution profile $\rho(r)$ of ovispirin proteins with respect to AuNP surface in the case of 3.2 nm AuNP. The $\rho(r)$ profile was computed using 100 configurations containing the last 100 ns CGMD simulations. The top position of the AuNP surface locates at 1.6 nm; the onset of the $\rho(r)$ peaks at 1.75 nm, and the peak position at 2.15 nm.

where n is the number of protein CG beads located at the distance r in a shell of thickness dr. The center-of-mass of each NP serves as the reference point for obtaining the $\rho(r)$ profile. As shown in Figure 2, in the bulk (r > 6 nm), the protein density does not reach zero value (Figure 2), which also suggests that not all ovispirin proteins were adsorbed (Figure 1c). A significant density peak locates around r ∼ 2.15 nm (Figure 2), which indicates a condensed protein adsorption layer with a thickness of ∼3.45 nm. This result, along with the visual inspection, consistently demonstrates that the multilayered adsorption of ovispirin proteins on the AuNPs is negligible.

https://dx.doi.org/10.1021/acs.langmuir.0c02767
Langmuir 2020, 36, 13356−13363

To understand the composition of the adsorbed protein layers on the 3.2 nm AuNP surface, we quantified the NP surface chemistry by monitoring the number of amino residues on the nanoparticle surface. The number N of a residue was computed via $N = N_{bead}/N_r$, where N_{bead} is the bead number of a residue within the cutoff distance (r < 2.15 nm), which corresponds to the peak position of the density profile in Figure 2, whereas N_r is the number of this residue type according to the MARTINI force field.

As Figure 3 shows, eight types of residues are in direct contact with the AuNP surface. These residues belong to different categories in hydrophobicity index[61] at pH 7, including hydrophilic residues (LYS, ARG, and ASN), neutral residues (HIS and GLY), and hydrophobic residues (TYR, ILE, and LEU). The top four residues on AuNPs include both hydrophobic (TYR and ILE) and hydrophilic (LYS and ARG) residues (Figure 3). The presence of hydrophobic residues is expected due to the hydrophobic nature of the AuNP, while that of hydrophilic residues on the surface implies that the protein−protein interactions also contribute to the adsorption process.

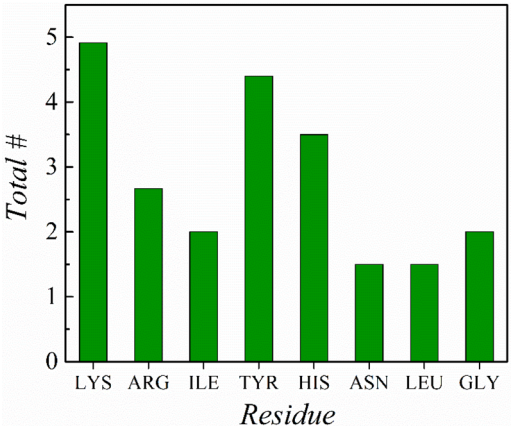

Figure 3. Number N of ovispirin residues in direct contact with the AuNP surface within the cutoff distance, r < 2.15 nm.

The adsorption orientation is quantified with an angle θ between a radial vector and a vector defined by a regression line through the beads' points for each protein (Figure 4a). The former vector connects the center-of-mass of the AuNPs and the centroid of the protein. The latter also goes through the centroid but in the direction from a protein's N-terminus to C-terminus as determined by the singular value decomposition in three dimensions. When an ovispirin protein lies down on the surface, its θ is around 90°, while for a upright ovispirin, its θ is close to either 0° or 180°. Figure 4b shows that on the surface of a larger-sized, 10 nm NP, almost all proteins lie down on the surface with $\theta \sim 90°$. However, on the surface of the smaller, 3.2 nm NP, there is a much broader distribution in the θ profile, which demonstrates that the proteins can either stand up or lie down on the 3.2 nm NP surface. Also, the percentage of ovispirn with the angle close to 180° is higher than that near 0°, indicating that the adsorption through the C-terminus (of GLY) is favorable compared to that via the N-terminus (of LYS).

This significant difference in the θ profile implies an increase in the NP size (i.e., a decrease in the NP curvature) and can enhance ovispirin protein−surface interactions. The observations of large-scale CGMD simulations in this work are consistent with the findings of our previous study of single-protein adsorption, using atomistic MD simulation and free energy computation,[35] in that both protein−surface interactions and the surface−solvent short-range hydrophobicity effect, i.e., $\gamma\Delta A$ (γ standing for the surface tension and ΔA for the available surface area) are driving forces of protein adsorption on a neutral hydrophobic surface. Given enough surface area, a protein is more likely to lie down on a hydrophobic surface with large surface tension.[35] In our CGMD simulations, the main characteristic of surface hydrophobicity was described with the MATRINI force field,[45] and the small effect of metallic gold surface polarization[30] upon protein adsorption was neglected. As nanoparticle diameter decreases, the total amount of surface atoms decreases, and the exposed surface area becomes smaller, which reduces the protein−surface interactions and weakens the substrate surface hydrophobic effect, resulting in different orientations of the adsorbed proteins. Different from our previous study of single-protein adsorption,[30,31,35] this work involves multiple proteins. The electrostatic interactions among charged proteins also play a key role in protein adsorption, i.e., the protein corona formation. It is worth mentioning that the size-dependent orientation distribution of the adsorbed proteins on nanoparticle surfaces is different from the conventional random-sequence theory.[62] The theory has been widely applied to modeling protein adsorption on a flat surface at the macroscopic level, assuming the same adsorption orientation on a flat substrate surface and taking into consideration the steric effect on packing (i.e., the jamming packing limit) on the available two-dimension adsorption

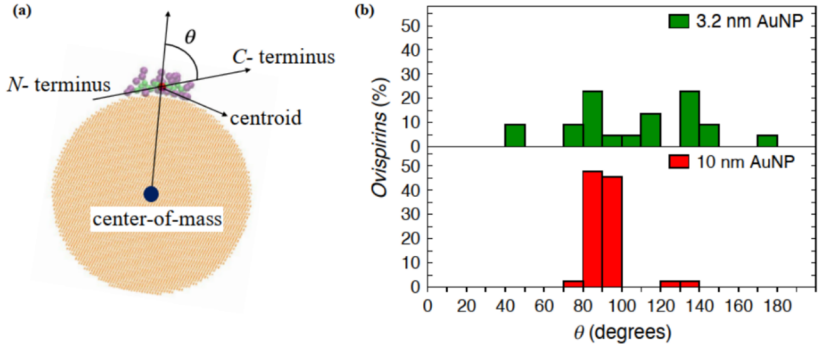

Figure 4. Orientation distribution profile of ovispirin proteins with respect to the AuNP surface: (a) a snapshot of the definition of protein adsorption orientation angle θ; (b) the distribution of θ for proteins on 3.2 and 10 nm AuNP surfaces.

https://dx.doi.org/10.1021/acs.langmuir.0c02767
Langmuir 2020, 36, 13356−13363

surface area due to the protein shape.[62] Our study will pave the road for future theoretical modeling and the clarification of the experimental data.

Formation and Structure of Lysozyme Protein Corona. To compare with the smaller-sized ovispirin protein, the dynamic processes of lysozyme corona formation on 3.2 and 10 nm AuNPs were examined using the same mass concentration method. Similar to the simulations of ovispirin, lysozyme proteins were initially dispersed in the bulk water (Figure 5a,d). Figure 5 summarizes the dynamics of the formation of lysozyme corona. Unlike ovispirin, more lysozyme proteins clustered in the bulk, even prior to the onset of the adsorption throughout the simulation process in both AuNP cases (Figure 5b,e). Within 1.2 μs, all lysozyme proteins were adsorbed onto the 10 nm AuNP, whereas for 3.2 nm AuNPs, it took ~2 μs. As the NP size decreased, the lysozyme proteins formed larger-sized protein aggregates attached to the nanoparticles (Figure 5c,f). This is likely a result of the larger surface on the 10 nm NPs, where more proteins have a greater chance of coming into direct contact with the AuNP surface. The packing of the protein corona was inhomogeneous, with a large space remaining empty on the nanoparticle. As shown in Figure S1 in Supporting Information, we doubled the protein concentration. Protein aggregates were also observed on the surfaces of both NPs. Our simulation results are in agreement with the findings of previous experiments in the literature,[63] which showed that an AuNP could induce the aggregation of lysozyme proteins. It is also noteworthy that in our CGMD simulations of both ovispirin and lysozyme proteins within the time scale of a few microseconds, we did not detect a scenario in which a preadsorbed protein was kicked away from the surface and replaced by another protein. Such a step of replacing/exchanging has been assumed as one of the key steps in the modeling of protein adsorption kinetics at the macroscopic level.[64−66]

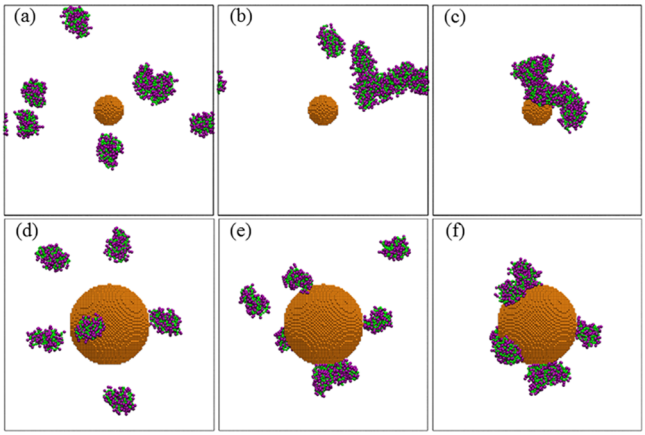

Figure 5. Dynamic processes of lysozyme corona formation. In the case of 3.2 nm AuNPs: (a) the initial configuration, (b) the configuration at t = 1 μs, and (c) the final configuration at t = 3.8 μs; in the case of 10 nm AuNPs: (d) the initial configuration, (e) the configuration at t = 1 μs, and (f) the final configuration at t = 3.8 μs.

Structural Change of Adsorbed Ovispirin Proteins. To study protein structural changes, 100 ns atomistic MD simulations were performed for the case of ovispirin adsorption on the 10 nm AuNPs, using the final configuration obtained with CGMD as the initial input. In CGMD simulations, all ovispirin proteins were adsorbed onto the surface. Figure 6 summarizes the averaged secondary structure of all adsorbed proteins in the configuration of the last 5 ns in comparison with the protein crystal structure. DSSP (database of secondary structure assignments)[67] was used to assign the secondary structures. Figure 6a shows the ovispirin protein initial crystal structure, which includes two secondary structure types: 82% α-helix and 18% coil. However, the averaged structure of ovispirin proteins in the corona was randomized and turned into six types: 5-helix, 3-helix, α-helix, turn, bend, and coil. Significant changes were noticeable for both helix and coil. The percentage of coil increased to an estimated amount of 34%, whereas that of the helix decreased to a final amount of 19%. The loss of protein structures also indicates strong protein−surface interactions.

We monitored the secondary structure of each adsorbed protein. As shown in Figure 6b, the protein structures in different local areas are quite different from each other. Some proteins are totally or mostly randomized, whereas others still maintain a certain percentage of helix structure. For demonstration purposes (Figure 7), we showed the secondary structural evolution of two separated ovispirins. One of them shows that the helical structure was totally randomized (Figure 7(a)), while the other is still able to maintain some of its helix structure (Figure 7(b)). The difference can be attributed to the slight difference in the protein residues, which are in direct contact with the AuNP surface, and also to the difference in local structure, and protein−protein interactions. Experimental measurements using circular dichroism (CD),[68] Fourier transform infrared (FTIR) spectroscopy[12,69] or surface-

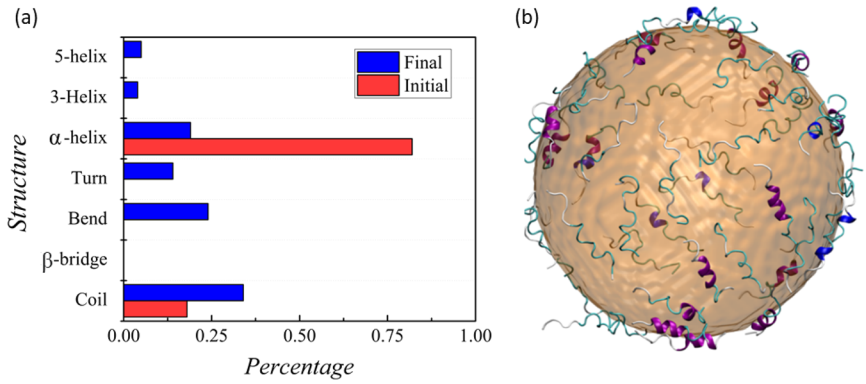

Figure 6. (a) Averaged secondary structure of the adsorbed ovispirin proteins on the 10 nm Au surface in comparison with the protein crystal structure; (b) a snapshot of the final configuration of proteins on the AuNP surfaces.

https://dx.doi.org/10.1021/acs.langmuir.0c02767
Langmuir 2020, 36, 13356−13363

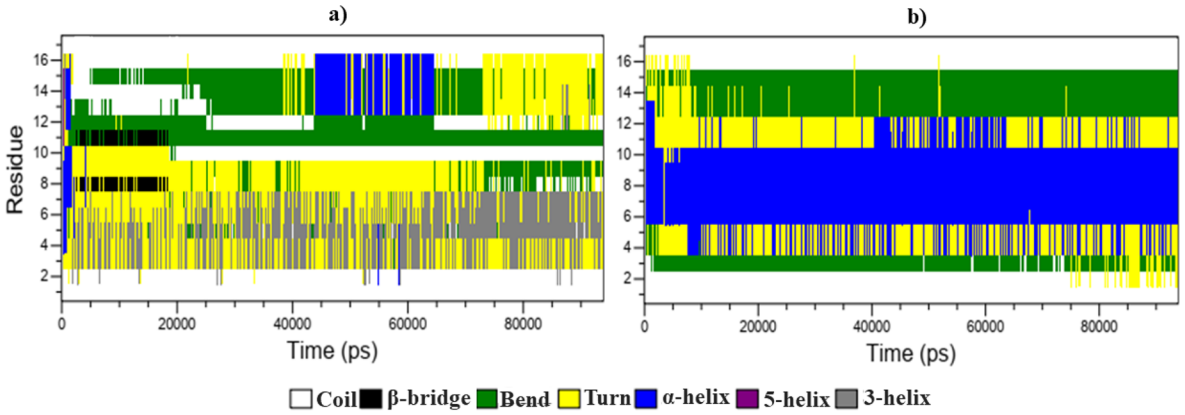

Figure 7. Time evolution of secondary structure of two different adsorbed ovispirins. DSSP algorithm[67] was used to define the secondary structure.

enhanced Raman spectroscopy (SERS)[63] can only measure the overall average secondary structures.

DISCUSSION AND CONCLUSION

Multiple proteins adsorbed on nanoparticles give rise to protein corona, alter the NP surface chemicophysical properties, and affect their performance in applications. Our fundamental study of protein corona on bare gold nanoparticles will shed light on the future development of nanoparticle-based molecular sensing techniques of SERS and drug delivery. We performed large-scale CGMD simulations at the mesoscopic scale to study protein corona using model systems consisting of differently sized proteins (ovispirin and lysozyme) and AuNPs. A bare AuNP was utilized as an ideal hydrophobic model. Our mesoscopic simulations demonstrated the formation processes and structures of protein corona of two different proteins. The study in this work offers an insight into the dynamic process of protein adsorption on the nanoparticle surface, particularly at the early stage.

Our study showed that the process of multiple-protein adsorption, i.e., the formation of the protein corona, is more complex than that of single-protein adsorption. In addition to the surface hydrophobic effect and protein−surface interactions, other factors related to protein−protein interactions need to be taken into account. The protein corona structure is highly correlated with protein type and NP size.

More specifically, homogeneous protein corona with a single-layer packing structure was detected for the smaller ovispirin protein due to stronger protein−surface interactions. However, multilayered lysozyme protein aggregates were observed on a gold nanoparticle with an inhomogeneous packing structure, indicating stronger protein−protein interactions. The size of nanoparticles has more influence on the adsorption orientations of ovispirin proteins inside the single-layered protein corona than on lysozyme aggregates.

Further atomistic MD simulations of ovispirin proteins on the AuNP surface were carried out to complement the CGMD simulations. The atomistic simulations demonstrated large alterations of protein secondary structure and suggested an inhomogeneous local structure. Our simulation observation of the heterogeneity in the local structure of protein corona has extremely important implications for increasing the efficiency of drug delivery and the accuracy of biosensing technologies.

ASSOCIATED CONTENT

Supporting Information

The Supporting Information is available free of charge at https://pubs.acs.org/doi/10.1021/acs.langmuir.0c02767.

Dynamic processes of lysozyme corona formation (Figure S1a−f) on AuNPs of two different sizes (3.2 and 10 nm) (PDF)

AUTHOR INFORMATION

Corresponding Authors

Yong Wei − *Department of Computer Science and Information Systems, University of North Georgia, Dahlonega, Georgia 30597, United States*; Email: yong.wei@ung.edu

Xiuping Tao − *Department of Chemistry, Winston-Salem State University, Winston-Salem, North Carolina 27110, United States*; Email: taoxi@wssu.edu

Tao Wei − *Department of Chemical Engineering, Howard University, Washington, D.C. 20059, United States*; orcid.org/0000-0001-6888-1658; Email: tao.wei@howard.edu

Authors

Md Symon Jahan Sajib − *Department of Chemical Engineering, Howard University, Washington, D.C. 20059, United States*

Pranab Sarker − *Department of Chemistry, Winston-Salem State University, Winston-Salem, North Carolina 27110, United States*

Complete contact information is available at: https://pubs.acs.org/10.1021/acs.langmuir.0c02767

Notes

The authors declare no competing financial interest.

ACKNOWLEDGMENTS

T. Wei and X. Tao acknowledge the grant support from National Science Foundation (NSF 1831559). T. Wei is grateful for computational resources from the program of Extreme Science and Engineering Discovery Environment (XSEDE) and the Texas Advanced Computing Center (TACC).

REFERENCES

(1) Rösch, N.; Pacchioni, G. Electronic Structures of Metal Clusters and Cluster Compounds. *Clusters and Colloids: From Theory to Applications*; VCH Verlagsgesellschaft mbH, 1994; pp 5−88.

(2) Ghosh, S. K.; Kundu, S.; Mandal, M.; Pal, T. Silver and gold nanocluster catalyzed reduction of methylene blue by arsine in a micellar medium. *Langmuir* **2002**, *18* (23), 8756−8760.
(3) Ghosh, S. K.; Pal, A.; Kundu, S.; Nath, S.; Pal, T. Fluorescence quenching of 1-methylaminopyrene near gold nanoparticles: size regime dependence of the small metallic particles. *Chem. Phys. Lett.* **2004**, *395* (4−6), 366−372.
(4) Ghosh, S. K.; Pal, A.; Nath, S.; Kundu, S.; Panigrahi, S.; Pal, T. Dimerization of eosin on nanostructured gold surfaces: Size regime dependence of the small metallic particles. *Chem. Phys. Lett.* **2005**, *412* (1−3), 5−11.
(5) Kubo, R. Electronic properties of metallic fine particles. I. *J. Phys. Soc. Jpn.* **1962**, *17* (6), 975−986.
(6) Casalini, T.; Limongelli, V.; Schmutz, M.; Som, C.; Jordan, O.; Wick, P.; Borchard, G.; Perale, G. Molecular modeling for nanomaterials-biology interactions: opportunities, challenges and perspectives. *Front. Bioeng. Biotechnol.* **2019**, *7*, 268.
(7) Cedervall, T.; Lynch, I.; Foy, M.; Berggård, T.; Donnelly, S. C.; Cagney, G.; Linse, S.; Dawson, K. A. Detailed identification of plasma proteins adsorbed on copolymer nanoparticles. *Angew. Chem., Int. Ed.* **2007**, *46* (30), 5754−5756.
(8) Cedervall, T.; Lynch, I.; Lindman, S.; Berggård, T.; Thulin, E.; Nilsson, H.; Dawson, K. A.; Linse, S. Understanding the nanoparticle-protein corona using methods to quantify exchange rates and affinities of proteins for nanoparticles. *Proc. Natl. Acad. Sci. U. S. A.* **2007**, *104* (7), 2050−2055.
(9) Lundqvist, M.; Stigler, J.; Elia, G.; Lynch, I.; Cedervall, T.; Dawson, K. A. Nanoparticle size and surface properties determine the protein corona with possible implications for biological impacts. *Proc. Natl. Acad. Sci. U. S. A.* **2008**, *105* (38), 14265−14270.
(10) Dell'Orco, D.; Lundqvist, M.; Oslakovic, C.; Cedervall, T.; Linse, S. Modeling the time evolution of the nanoparticle-protein corona in a body fluid. *PLoS One* **2010**, *5* (6), No. e10949.
(11) Jiang, S.; Cao, Z. Ultralow-fouling, functionalizable, and hydrolyzable zwitterionic materials and their derivatives for biological applications. *Adv. Mater.* **2010**, *22* (9), 920−932.
(12) Wei, T.; Kaewtathip, S.; Shing, K. Buffer effect on protein adsorption at liquid/solid interface. *J. Phys. Chem. C* **2009**, *113* (6), 2053−2062.
(13) Tsai, W. B.; Grunkemeier, J. M.; Horbett, T. A. Human plasma fibrinogen adsorption and platelet adhesion to polystyrene. *J. Biomed. Mater. Res.* **1999**, *44* (2), 130−139.
(14) Casals, E.; Pfaller, T.; Duschl, A.; Oostingh, G. J.; Puntes, V. Time evolution of the nanoparticle protein corona. *ACS Nano* **2010**, *4* (7), 3623−3632.
(15) Petryayeva, E.; Krull, U. J. Localized surface plasmon resonance: Nanostructures, bioassays and biosensing—A review. *Anal. Chim. Acta* **2011**, *706* (1), 8−24.
(16) Kong, F.-Y.; Zhang, J.-W.; Li, R.-F.; Wang, Z.-X.; Wang, W.-J.; Wang, W. Unique roles of gold nanoparticles in drug delivery, targeting and imaging applications. *Molecules* **2017**, *22* (9), 1445.
(17) van Zoelen, W.; Buss, H. G.; Ellebracht, N. C.; Lynd, N. A.; Fischer, D. A.; Finlay, J.; Hill, S.; Callow, M. E.; Callow, J. A.; Kramer, E. J.; et al. Sequence of hydrophobic and hydrophilic residues in amphiphilic polymer coatings affects surface structure and marine antifouling/fouling release properties. *ACS Macro Lett.* **2014**, *3* (4), 364−368.
(18) Leonardi, A. K.; Ober, C. K. Polymer-based marine antifouling and fouling release surfaces: strategies for synthesis and modification. *Annu. Rev. Chem. Biomol. Eng.* **2019**, *10*, 241−264.
(19) Schultz, M.; Bendick, J.; Holm, E.; Hertel, W. Economic impact of biofouling on a naval surface ship. *Biofouling* **2011**, *27* (1), 87−98.
(20) Zhu, Y.-X.; Jia, H.-R.; Pan, G.-Y.; Ulrich, N. W.; Chen, Z.; Wu, F.-G. Development of a light-controlled nanoplatform for direct nuclear delivery of molecular and nanoscale materials. *J. Am. Chem. Soc.* **2018**, *140* (11), 4062−4070.
(21) Mirshafiee, V.; Mahmoudi, M.; Lou, K.; Cheng, J.; Kraft, M. L. Protein corona significantly reduces active targeting yield. *Chem. Commun.* **2013**, *49* (25), 2557−2559.
(22) Tenzer, S.; Docter, D.; Kuharev, J.; Musyanovych, A.; Fetz, V.; Hecht, R.; Schlenk, F.; Fischer, D.; Kiouptsi, K.; Reinhardt, C.; et al. Rapid formation of plasma protein corona critically affects nanoparticle pathophysiology. *Nat. Nanotechnol.* **2013**, *8* (10), 772−781.
(23) Nguyen, V. H.; Lee, B.-J. Protein corona: a new approach for nanomedicine design. *Int. J. Nanomed.* **2017**, *12*, 3137.
(24) Rampado, R.; Crotti, S.; Caliceti, P.; Pucciarelli, S.; Agostini, M. Recent Advances in Understanding the Protein Corona of Nanoparticles and in the Formulation of "Stealthy" Nanomaterials. *Front. Bioeng. Biotechnol.* **2020**, *8*. DOI: 10.3389/fbioe.2020.00166
(25) Carrillo-Carrion, C.; Carril, M.; Parak, W. J. Techniques for the experimental investigation of the protein corona. *Curr. Opin. Biotechnol.* **2017**, *46*, 106−113.
(26) Del Pino, P.; Pelaz, B.; Zhang, Q.; Maffre, P.; Nienhaus, G. U.; Parak, W. J. Protein corona formation around nanoparticles-from the past to the future. *Mater. Horiz.* **2014**, *1* (3), 301−313.
(27) Lundqvist, M.; Augustsson, C.; Lilja, M.; Lundkvist, K.; Dahlbäck, B.; Linse, S.; Cedervall, T. The nanoparticle protein corona formed in human blood or human blood fractions. *PLoS One* **2017**, *12* (4), No. e0175871.
(28) Wei, T.; Sajib, M. S. J.; Samieegohar, M.; Ma, H.; Shing, K. Self-Assembled Monolayers of an Azobenzene Derivative on Silica and Their Interactions with Lysozyme. *Langmuir* **2015**, *31* (50), 13543−13552.
(29) Samieegohar, M.; Ma, H.; Sha, F.; Jahan Sajib, M. S.; Guerrero-García, G. I.; Wei, T. Understanding the interfacial behavior of lysozyme on Au (111) surfaces with multiscale simulations. *Appl. Phys. Lett.* **2017**, *110* (7), 073703.
(30) Zhang, T.; Wei, T.; Han, Y.; Ma, H.; Samieegohar, M.; Chen, P.-W.; Lian, I.; Lo, Y.-H. Protein-ligand interaction detection with a novel method of transient induced molecular electronic spectroscopy (TIMES): experimental and theoretical studies. *ACS Cent. Sci.* **2016**, *2* (11), 834−842.
(31) Wei, T.; Ma, H.; Nakano, A. Decaheme cytochrome MtrF adsorption and electron transfer on gold surface. *J. Phys. Chem. Lett.* **2016**, *7* (5), 929−936.
(32) Wei, T.; Carignano, M. A.; Szleifer, I. Lysozyme adsorption on polyethylene surfaces: why are long simulations needed? *Langmuir* **2011**, *27* (19), 12074−12081.
(33) Wei, T.; Carignano, M. A.; Szleifer, I. Molecular dynamics simulation of lysozyme adsorption/desorption on hydrophobic surfaces. *J. Phys. Chem. B* **2012**, *116* (34), 10189−10194.
(34) Jahan Sajib, M. S.; Wei, Y.; Mishra, A.; Zhang, L.; Nomura, K.-i.; Kalia, R. K.; Vashishta, P.; Nakano, A.; Murad, S.; Wei, T. Atomistic Simulations of Biofouling and Molecular Transfer of Crosslinked Aromatic Polyamide Membrane for Desalination. *Langmuir* **2020**, *36* (26), 7658−7668.
(35) Nakano, C. M.; Ma, H.; Wei, T. Study of lysozyme mobility and binding free energy during adsorption on a graphene surface. *Appl. Phys. Lett.* **2015**, *106* (15), 153701.
(36) Zheng, J.; Li, L.; Tsao, H.-K.; Sheng, Y.-J.; Chen, S.; Jiang, S. Strong repulsive forces between protein and oligo (ethylene glycol) self-assembled monolayers: a molecular simulation study. *Biophys. J.* **2005**, *89* (1), 158−166.
(37) Liu, Y.; Zhang, Y.; Ren, B.; Sun, Y.; He, Y.; Cheng, F.; Xu, J.; Zheng, J. Molecular Dynamics Simulation of the Effect of Carbon Space Lengths on the Antifouling Properties of Hydroxyalkyl Acrylamides. *Langmuir* **2019**, *35* (9), 3576−3584.
(38) Kmiecik, S.; Gront, D.; Kolinski, M.; Wieteska, L.; Dawid, A. E.; Kolinski, A. Coarse-grained protein models and their applications. *Chem. Rev.* **2016**, *116* (14), 7898−7936.
(39) Voth, G. A. *Coarse-graining of condensed phase and biomolecular systems*; CRC Press, 2008.
(40) Lin, X.; Bai, T.; Zuo, Y. Y.; Gu, N. Promote potential applications of nanoparticles as respiratory drug carrier: insights from molecular dynamics simulations. *Nanoscale* **2014**, *6* (5), 2759−2767.
(41) Quan, X.; Peng, C.; Zhao, D.; Li, L.; Fan, J.; Zhou, J. Molecular understanding of the penetration of functionalized gold nanoparticles into asymmetric membranes. *Langmuir* **2017**, *33* (1), 361−371.

(42) Yu, G.; Zhou, J. Understanding the curvature effect of silica nanoparticles on lysozyme adsorption orientation and conformation: a mesoscopic coarse-grained simulation study. *Phys. Chem. Chem. Phys.* **2016**, *18* (34), 23500−23507.
(43) Lopez, H.; Lobaskin, V. Coarse-grained model of adsorption of blood plasma proteins onto nanoparticles. *J. Chem. Phys.* **2015**, *143* (24), 243138.
(44) Tavanti, F.; Pedone, A.; Menziani, M. C. A closer look into the ubiquitin corona on gold nanoparticles by computational studies. *New J. Chem.* **2015**, *39* (4), 2474−2482.
(45) Marrink, S. J.; Risselada, H. J.; Yefimov, S.; Tieleman, D. P.; De Vries, A. H. The MARTINI force field: coarse grained model for biomolecular simulations. *J. Phys. Chem. B* **2007**, *111* (27), 7812−7824.
(46) Huang, J.; Rauscher, S.; Nawrocki, G.; Ran, T.; Feig, M.; de Groot, B. L.; Grubmüller, H.; MacKerell, A. D. CHARMM36m: an improved force field for folded and intrinsically disordered proteins. *Nat. Methods* **2017**, *14* (1), 71−73.
(47) Abraham, M. J.; Murtola, T.; Schulz, R.; Páll, S.; Smith, J. C.; Hess, B.; Lindahl, E. GROMACS: High performance molecular simulations through multi-level parallelism from laptops to supercomputers. *SoftwareX* **2015**, *1*, 19−25.
(48) Wassenaar, T. A.; Pluhackova, K.; Böckmann, R. A.; Marrink, S. J.; Tieleman, D. P. Going backward: a flexible geometric approach to reverse transformation from coarse grained to atomistic models. *J. Chem. Theory Comput.* **2014**, *10* (2), 676−690.
(49) Souza, P. C. T.; Marrink, S. J. Martini 3 - Open Beta-Release, http://cgmartini.nl, 2020.
(50) Daniel, M.-C.; Astruc, D. Gold nanoparticles: assembly, supramolecular chemistry, quantum-size-related properties, and applications toward biology, catalysis, and nanotechnology. *Chem. Rev.* **2004**, *104* (1), 293−346.
(51) Gupta, R.; Rai, B. Effect of size and surface charge of gold nanoparticles on their skin permeability: a molecular dynamics study. *Sci. Rep.* **2017**, *7* (1), 1−13.
(52) Gupta, R.; Rai, B. Penetration of gold nanoparticles through human skin: unraveling its mechanisms at the molecular scale. *J. Phys. Chem. B* **2016**, *120* (29), 7133−7142.
(53) Song, B.; Yuan, H.; Jameson, C. J.; Murad, S. Role of surface ligands in nanoparticle permeation through a model membrane: a coarse-grained molecular dynamics simulations study. *Mol. Phys.* **2012**, *110* (18), 2181−2195.
(54) Sridhar, D. B.; Gupta, R.; Rai, B. Effect of surface coverage and chemistry on self-assembly of monolayer protected gold nanoparticles: a molecular dynamics simulation study. *Phys. Chem. Chem. Phys.* **2018**, *20* (40), 25883−25891.
(55) Lin, J.; Zhang, H.; Chen, Z.; Zheng, Y. Penetration of lipid membranes by gold nanoparticles: insights into cellular uptake, cytotoxicity, and their relationship. *ACS Nano* **2010**, *4* (9), 5421−5429.
(56) Hossain, S. I.; Gandhi, N. S.; Hughes, Z. E.; Saha, S. C. The role of SP-B 1−25 peptides in lung surfactant monolayers exposed to gold nanoparticles. *Phys. Chem. Chem. Phys.* **2020**, *22* (27), 15231−15241.
(57) Bussi, G.; Donadio, D.; Parrinello, M. Canonical sampling through velocity rescaling. *J. Chem. Phys.* **2007**, *126* (1), 014101.
(58) Heinz, H.; Vaia, R.; Farmer, B.; Naik, R. Accurate simulation of surfaces and interfaces of face-centered cubic metals using 12- 6 and 9- 6 Lennard-Jones potentials. *J. Phys. Chem. C* **2008**, *112* (44), 17281−17290.
(59) Heinz, H.; Farmer, B. L.; Pandey, R. B.; Slocik, J. M.; Patnaik, S. S.; Pachter, R.; Naik, R. R. Nature of molecular interactions of peptides with gold, palladium, and Pd- Au bimetal surfaces in aqueous solution. *J. Am. Chem. Soc.* **2009**, *131* (28), 9704−9714.
(60) Ali, M. R.; Wu, Y.; Ghosh, D.; Do, B. H.; Chen, K.; Dawson, M. R.; Fang, N.; Sulchek, T. A.; El-Sayed, M. A. Nuclear membrane-targeted gold nanoparticles inhibit cancer cell migration and invasion. *ACS Nano* **2017**, *11* (4), 3716−3726.
(61) Monera, O. D.; Sereda, T. J.; Zhou, N. E.; Kay, C. M.; Hodges, R. S. Relationship of sidechain hydrophobicity and α-helical propensity on the stability of the single-stranded amphipathic α-helix. *J. Pept. Sci.* **1995**, *1* (5), 319−329.
(62) Talbot, J.; Tarjus, G.; Van Tassel, P.; Viot, P. From car parking to protein adsorption: an overview of sequential adsorption processes. *Colloids Surf., A* **2000**, *165* (1−3), 287−324.
(63) Zhang, D.; Neumann, O.; Wang, H.; Yuwono, V. M.; Barhoumi, A.; Perham, M.; Hartgerink, J. D.; Wittung-Stafshede, P.; Halas, N. J. Gold nanoparticles can induce the formation of protein-based aggregates at physiological pH. *Nano Lett.* **2009**, *9* (2), 666−671.
(64) Rabe, M.; Verdes, D.; Seeger, S. Understanding protein adsorption phenomena at solid surfaces. *Adv. Colloid Interface Sci.* **2011**, *162* (1−2), 87−106.
(65) Lundström, I.; Elwing, H. Simple kinetic models for protein exchange reactions on solid surfaces. *J. Colloid Interface Sci.* **1990**, *136* (1), 68−84.
(66) Wahlgren, M.; Arnebrant, T.; Lundström, I. The adsorption of lysozyme to hydrophilic silicon oxide surfaces: comparison between experimental data and models for adsorption kinetics. *J. Colloid Interface Sci.* **1995**, *175* (2), 506−514.
(67) Kabsch, W.; Sander, C. Dictionary of protein secondary structure: pattern recognition of hydrogen-bonded and geometrical features. *Biopolymers* **1983**, *22* (12), 2577−2637.
(68) Laera, S.; Ceccone, G.; Rossi, F.; Gilliland, D.; Hussain, R.; Siligardi, G.; Calzolai, L. Measuring protein structure and stability of protein-nanoparticle systems with synchrotron radiation circular dichroism. *Nano Lett.* **2011**, *11* (10), 4480−4484.
(69) Tsai, D.-H.; DelRio, F. W.; Keene, A. M.; Tyner, K. M.; MacCuspie, R. I.; Cho, T. J.; Zachariah, M. R.; Hackley, V. A. Adsorption and conformation of serum albumin protein on gold nanoparticles investigated using dimensional measurements and in situ spectroscopic methods. *Langmuir* **2011**, *27* (6), 2464−2477.

https://dx.doi.org/10.1021/acs.langmuir.0c02767
Langmuir 2020, 36, 13356−13363